Mid-Infrared Energy Deposition Spectroscopy

Jiaze Yin,[1,2] Christian Pfluegl,[3] Chu C. Teng,[3] Rylie Bolarinho,[2,4] Guo Chen,[1,2] Xinrui Gong,[2,5] Dashan Dong,[1,2] Daryoosh Vakhshoori,[3] and Ji-Xin Cheng[1,2,4,5,*]

[1]*Department of Electrical and Computer Engineering, Boston University, Boston, Massachusetts 02215, USA*
[2]*Photonics Center, Boston University, Boston, Massachusetts 02215, USA*
[3]*Pendar Technologies, Cambridge, Massachusetts 02138, USA*
[4]*Department of Chemistry, Boston University, Boston, Massachusetts 02215, USA*
[5]*Department of Biomedical Engineering, Boston University, Boston, Massachusetts 02215, USA*

(Received 28 September 2024; revised 10 January 2025; accepted 5 February 2025; published 6 March 2025)

It is generally assumed that the spectral acquisition speed in photothermal spectroscopy is fundamentally limited by the thermal diffusion process. Here, we demonstrate midinfrared energy deposition (MIRED) spectroscopy that offers both microsecond-scale temporal resolution and submicron spatial resolution. In this approach, the photothermal process is optically probed while the infrared pulses from a quantum cascade laser array are rapidly tuned. Based on Newton's law of heating and cooling, the energy deposition is the first derivative of local temperature rise over time and gives the instantaneous absorption. By employing time-resolved measurement of transient energy deposition, the upper limit for spectrum encoding shifts to the vibrational relaxation level, which occurs on the picosecond scale. This method significantly increases the detection bandwidth while retaining the sensitivity and resolution benefits of photothermal detection.

DOI: 10.1103/PhysRevLett.134.093804

By pump-probe measurement of absorption-induced change (temperature, size, refractive index, etc.) in a specimen, photothermal spectroscopy is an extremely sensitive analytical tool down to single molecule sensitivity [1,2]. The initial development of photothermal spectroscopy in the 1970s detected weak overtone transitions in molecules [3]. To enable chemical imaging of nonfluorescent species, various photothermal microscopy techniques have been developed in recent years. Visible photothermal microscopy developed in the 1990s enabled label-free imaging of single gold nanoparticles down to a few nanometers in diameter [4]. In the early 2000s, the integration of atomic force microscopy and infrared (IR) spectroscopy allowed nanoscale examination of molecules in thin, dried specimens [5]. Recently developed midinfrared photothermal (MIP) microscopy [6], also called optically detected photothermal IR, have enabled submicron-resolution bond-selective imaging in aqueous environments [7]. Further innovations include imaging at video rate [8,9], breaking the visible diffraction limits [10,11], high-throughput camera-based widefield measurements [12–14], and volumetric imaging by optical photothermal tomography [15,16].

Despite the extremely high sensitivity and resolution offered by photothermal detection, achieving rapid spectral acquisition via photothermal spectroscopy has been considered a major obstacle. This limitation arises from the time needed for cooling during temperature modulation, which takes microseconds or longer. Consequently, even with an ultrafast wavelength-sweeping IR source and single pulse detection speed [8], the effective detection bandwidth is restricted to only hundreds of kilohertz per color. As shown in Fig. 1(a), MIP spectroscopy uses a single-color IR source to excite a narrow band per measurement. Acquiring a spectrum requires continuously tuning the IR laser and inducing multiple cycles of photothermal modulation, with speeds typically around 0.1 s per 100 cm^{-1} for a high-speed external cavity quantum cascade laser. In this Letter, we break this speed limitation by revisiting the photothermal process from the perspective of energy deposition. According to Newton's law of heating and cooling [17], the local temperature $T(t)$ of the absorber is the integration of heat flux during excitation, as shown in Eq. (1),

$$C\frac{dT}{dt} = \dot{Q}_{\text{abs}} - \dot{Q}_{\text{diffusion}}. \tag{1}$$

Here, C represents the heat capacity of the absorber, $\dot{Q}_{\text{diffusion}}$ denotes the heat dissipation term driven by the temperature difference between the absorber and its surroundings, and $\dot{Q}_{\text{abs}}$ corresponds to the energy deposited through absorption, calculated by the product of IR intensity I_{IR} and absorption coefficient $\sigma(\lambda)$:

$$\dot{Q}_{\text{abs}} = I_{\text{IR}}(\lambda)\sigma(\lambda). \tag{2}$$

One can observe that the absorption coefficient $\sigma(\lambda)$ exists in the slope of the heating process instead of the

*Contact author: jxcheng@bu.edu

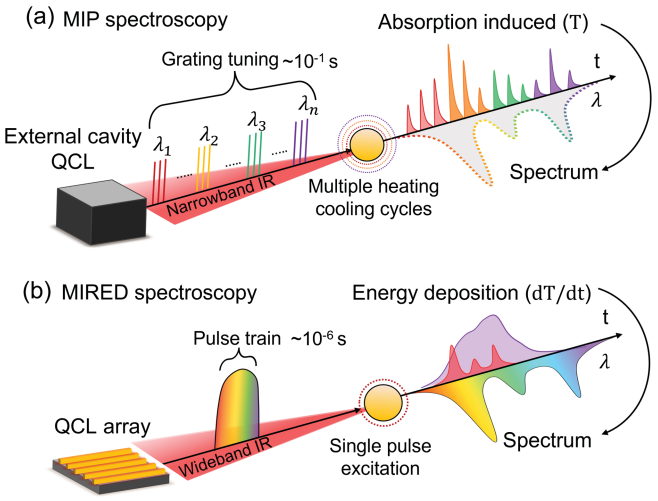

FIG. 1. Comparison of MIP spectroscopy and MIRED spectroscopy. (a) MIP signal is from a single-color excitation source. Measuring an absorption spectrum requires tuning IR wavelengths and involves multiple cycles of heating and cooling. (b) MIRED spectroscopy using a broadband excitation source. By performing time-resolved energy deposition measurement on a nanosecond scale, an absorption spectrum is obtained from the first derivative of local temperature rise.

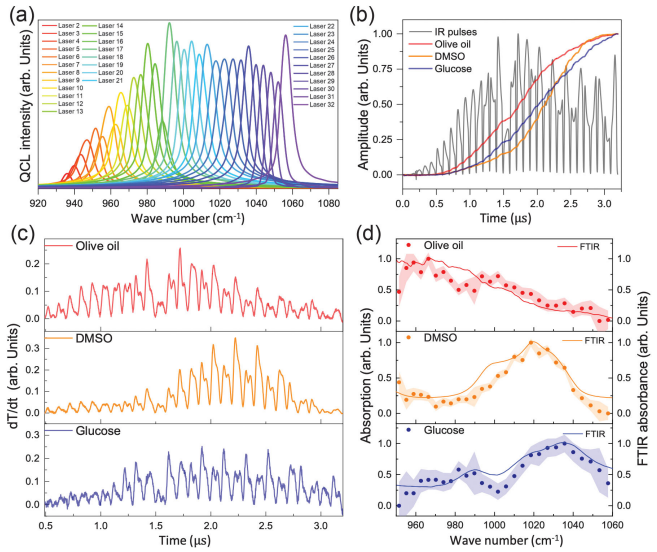

FIG. 2. MIRED spectra of olive oil, dimethyl sulfoxide (DMSO), and glucose solution. (a) Characterized power spectrum of QCL array. (b) Pulse train fired by QCLs array (gray) and induced heating curve of olive oil (red), DMSO (orange), and glucose solution (blue). (c) Time-resolved energy deposition. (d) MIRED spectra after normalizing with IR energy. Twenty measurements are performed, and averaging results are displayed. In (d), the data are presented as the mean ± standard deviations. The FTIR spectra are shown as a solid line for comparison.

overall amplitude, as shown in Eq. (2). Thus, by employing a time-resolved measurement of transient energy deposition, the upper limit for spectrum encoding shifts to the vibrational relaxation level, which occurs on the picosecond scale [18,19]. This approach enhances the detection bandwidth while preserving the sensitivity advantages of photothermal detection.

To demonstrate the concept, we developed MIRED spectroscopy utilizing broadband pulse train emissions from a beam-combined monolithic distributed-feedback quantum cascade laser (QCL) array [20,21]. Technically, the broadband IR source sequentially excites different molecular bands, as illustrated in Fig. 1(b). Time-resolved measurements are conducted during the excitation process, and the absorption spectrum is obtained from the transient energy deposition by calculating the time derivative of the heating curve. Spectrum acquisition is completed within the duration of the wideband pulse firing, which occurs on the microsecond scale. The theoretical framework of MIRED spectroscopy is outlined in the Supplemental Material (SM) [22] Note 1, with the experimental setup illustrated in Fig. S1. The contrast mechanism utilized in this setup is depicted in Fig. S2 and described in SM Note 2. In summary, the employed QCL array consists of 32 independent lasers, spaced 4 cm^{-1} apart, covering a range from 940 to 1056 cm^{-1}. Each laser emits a 100 ns-wide pulse, with all channels firing sequentially within 3.2 μs. The laser firing profile is characterized in Fig. S3, and the central wavenumbers, along with their corresponding powers, are listed in SM Table 1. The induced heating profile of the absorber is probed by a continuous-wave 532 nm laser. The probe is detected by a fast photodiode and digitized at 4 ns per point, providing the necessary temporal resolution to resolve the energy deposition from each individual laser pulse.

To validate the spectral fidelity, MIRED spectra of three different chemicals were measured, as presented in Fig. 2. The power spectrum of the QCL array is shown in Fig. 2(a). The time-resolved heating curves under excitation, normalized to the same amplitude scale for comparison, are displayed in Fig. 2(b). The energy deposition was then calculated by taking the time derivative of the heating curves, as shown in Fig. 2(c). This analysis reveals both the shape of each laser pulse and the relative absorption. Finally, the time-domain energy deposition data was converted into spectra, as illustrated in Fig. 2(d). Fourier-transform infrared (FTIR) spectra in solid lines (full spectra shown in Fig. S4) are provided for comparison, validating the MIRED results. In this window, the olive oil displays a peak at 966 cm^{-1} from the $-HC=CH-$ bending, dimethyl sulfoxide (DMSO) displays a strong absorption peak at 1022 cm^{-1} from the $S=O$ stretching, while the glucose solution with a concentration of 200 mg/dL shows a broader peak around 1035 cm^{-1} from the C-O stretching. It is important to note that the heat flux measured by taking the derivative of the temperature includes contributions from both absorption ($\dot{Q}_{abs}$) and diffusion ($\dot{Q}_{diffusion}$). For the sample measured above, the

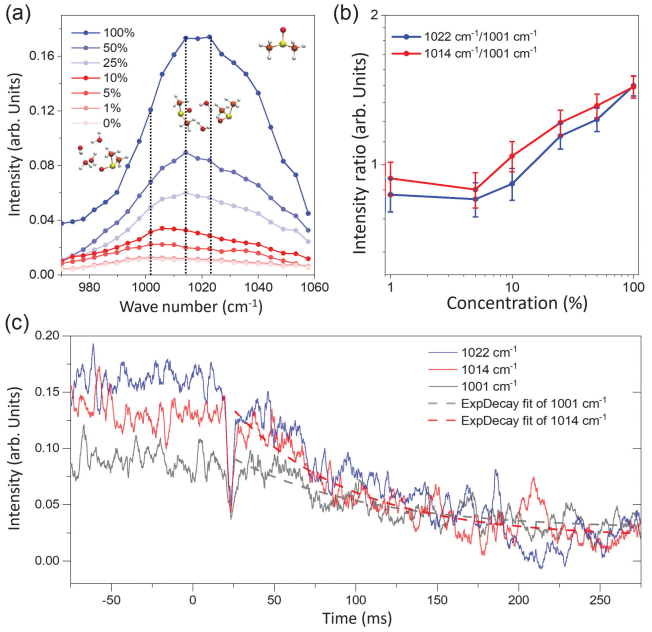

FIG. 3. MIRED spectroscopy of solvation dynamics on the microsecond scale. (a) MIRED spectrum of DMSO-water binary mixture at different DMSO ratios. (b) MIRED intensity ratio between two wave numbers versus DMSO concentration. Fifty measurements were performed, and the averaged results are displayed. The data are presented as the mean ± standard deviation. (c) DMSO-water mixing dynamics revealed by single pulse MIRED spectroscopy. 200 μL DI water is added to 10 μL DMSO by pipette at $t = 0$. The exponential decay is fit on the intensity at 1014 cm^{-1} and 1001 cm^{-1}. The time constants are 79 and 103 ms, respectively.

thermal diffusion rate is relatively slow compared to the excitation process. Consequently, $\dot{Q}_{\text{diffusion}}$ has a negligible impact on the MIRED spectra. This approximation is further discussed in SM Note 3. For objects with significantly faster heat diffusion rates, such as small particles, the MIRED scheme remains applicable for retrieving spectral information by incorporating a correction term into the measurement, as detailed in SM Note 4.

To demonstrate the microsecond-scale capabilities of MIRED spectroscopy, we conducted a continuous spectral acquisition to observe the rapid mixing process of DMSO and water. DMSO and water mixtures exhibit interesting physical properties, such as their dramatically changed freezing point and viscosity [25], attributed to the formation of molecular clusters through hydrogen-bond networks [26]. Given the IR sensitivity to bond vibrations, MIRED spectroscopy can distinguish cluster states and their populations. Steady-state MIRED spectra of various concentrations of DMSO solution are shown in Fig. 3(a). By reducing the percentage of DMSO, a redshift of the peak from 1022 cm^{-1} to 1001 cm^{-1} and decreased absorption can be observed. A similar red shift is observed for FTIR measurement, as shown in Fig. S8. This is explained by the decreased S = O dipole due to the formation of clusters with nonchanged methyl group rocking [27]. We quantified the change in intensity ratio versus DMSO concentration, as shown in Fig. 3(b). The curve represents the intensity ratio between the S = O peak at 1022 cm^{-1}(blue), 1014 cm^{-1}(red), and the shift peak at 1001 cm^{-1}. The ratio is approximately 1.4 at 100% DMSO concentration and decreases to below 1 when the DMSO concentration is less than 10%, indicating a change in bond dipole in addition to the reduction in analyte concentration. The molecular dynamics experiments begin with 100% DMSO, followed by the addition of excess water (20 times the volume of DMSO). The MIRED spectra are recorded continuously during the mixing process at a rate of 20 μs each, as shown in Fig. 3(c). The recording speed is determined by the QCL array repetition rate of 50 kHz, as illustrated in Fig. S9. Time-resolved spectroscopy reveals the kinetics of molecular diffusion (k_S) and the rate of cluster population changes (k_C). These two processes are approximated using exponential population decay. The intensity at 1001 cm^{-1}, attributed to methyl rocking, is solely influenced by diffusion ($\tau_{1001} = k_S^{-1}$). Conversely, the S = O absorption drop at 1014 cm^{-1} is governed by both processes with a combined lifetime ($\tau_{1014} = (k_S + k_C)^{-1}$). By fitting the MIRED intensity at 1001 cm^{-1} and 1014 cm^{-1}, the measured lifetimes are 103 and 79 ms, respectively. Consequently, the rate of water-DMSO cluster population change (k_C) is determined to be 2.95 s^{-1}, corresponding to a lifetime of 338 ms. We note here that MIRED captures dynamics on the microsecond to millisecond scale, unlike picosecond molecular dynamics studied with ultrafast spectroscopy, which focuses on vibrational mode relaxations influenced by mixture ratios in static solutions [28]. Instead, time-resolved MIRED provides a macroscopic view of population dynamics, especially in diffusion-limited systems transitioning toward equilibration in a new state.

We further developed MIRED microscopy for high-speed spectroscopic imaging with submicron resolution. Firstly, we imaged biomolecules in fixed U87 cancer cells immersed in phosphate-buffered saline, as shown in Fig. 4. The MIRED spectra can differentiate between fatty acid esters and carbohydrates. During imaging, a piezo stage raster scans the sample while MIRED spectroscopy continuously records data. The spectrum at each pixel is averaged by 10 times, resulting in an effective pixel dwell time 200 μs. The overall intensity, representing the total absorption of the sample, is shown in Fig. 4(a). We evaluate specific absorption bands of the sample, as shown in Figs. 4(c) and 4(c). The merged image in Fig. 4(d) reveals the intracellular distribution difference between esters and carbohydrates. Interestingly, aside from the diffuse carbohydrates spread throughout the cell body, a bright carbohydrates aggregate is observed. This aggregate is distinct from lipid droplets, as indicated by the dashed line in Fig. 4(e). These carbohydrate aggregates are likely glycogen in brain cancer cells [29,30].

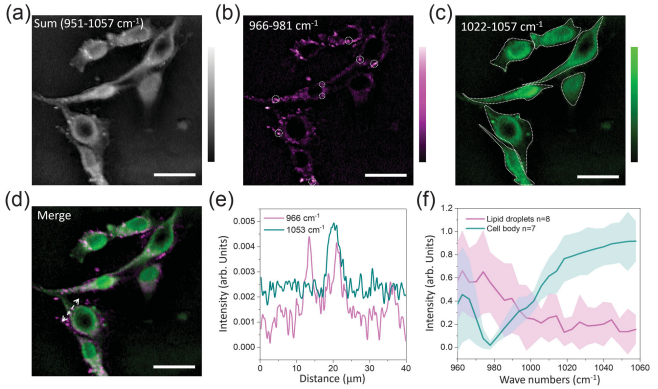

FIG. 4. MIRED spectroscopic imaging of fixed U87 cancer cells. (a) Average intensity from 951 to 1057 cm^{-1}. (b) Average intensity from 966 to 981 cm^{-1}; the lipid droplets show strong absorption. (c) Average intensity from 1022 to 1057 cm^{-1}; the carbohydrate contributes to the absorption. (d) Merge image of lipid ester (magenta), and carbohydrate (green). (e) Line profile of indicated area in merge image (d) reveals the carbohydrate aggregation. (f) The MIRED spectra of lipid droplets and cell body. N = 8, 6 accordingly for statistical analysis. The data are presented as the mean ± standard deviations.

The average spectra of the selected area indicated in Figs. 4(b) and 4(c) are shown in Fig. 4(f). The cancer cells cultured at delipidated (charcoal-striped) serum were measured, as shown in Fig. S10. A quantification analysis showed that the lipid depletion group had dropped intensity in the lipid channel from 966 to 981 cm^{-1} compared with the control group, while there was no significant change on the carbohydrate channel from 1022 to 1057 cm^{-1}, suggesting the accuracy of applying MIRED for mapping biomolecules. Additionally, single-color MIP imaging results obtained using an external cavity quantum cascade laser are provided for comparison in Fig. S11, confirming the carbohydrate peak observed in the MIRED experiment. It is worth noting that fixed cells were used in this Letter, but discussing phototoxicity in biological systems is essential for live-cell research. To this end, we performed time-resolved fluorescence thermometry on a DMSO sample, as shown in Fig. S12 and detailed in SM Note 5. This result revealed a transient temperature increase of 15.6 K during MIRED excitation and serves as an *in vitro* reference point for future investigations.

MIRED microscopy provides hyperspectral data with a single scan of the sample, significantly reducing the acquisition time for large tissue samples. We demonstrate mouse brain spectroscopic imaging as shown in Fig. S13, with pseudo colors red, green, and blue representing the average absorption from windows of 980–1010 cm^{-1}, 1018–1031 cm^{-1}, and 1035–1057 cm^{-1}, respectively. Structures such as the cerebrum, corpus callosum, and striatum are resolved [31] based on their chemical composition differences. The cerebrum is uniformly enriched with carbohydrates where the fatty acid ester channel (980–1010 cm^{-1}) is darker than the carbohydrate channel (1035–1057 cm^{-1}), indicating a high population of neurons and high carbohydrate levels in the brain. The corpus callosum is primarily composed of fiber bundles, showing strong absorption similar to fat. In between, the cerebral cortex region demonstrates a transition between the fat signal in white matter (inside the brain) and the relatively high sugar signal in gray matter.

In recent years, vibrational spectroscopy has been advanced in two major directions: increasing the speed to detect molecular processes in highly dynamic environments [32–36] and enhancing the sensitivity to visualize small amounts of substances in complex systems. In this Letter, we have developed MIRED-based vibrational spectroscopy and imaging methods that bridge these two directions. By measuring energy deposition via a pump-probe scheme, MIRED enables single-shot spectral acquisition on a microsecond timescale and imaging with submicron spatial resolution. This method opens a new way of using infrared spectroscopy to perform temporally and spatially resolved chemical analysis in various fields of material science and life science.

By revisiting the photothermal process, we find that the absorption coefficient can be accurately determined via time-resolved measurement of the heating slope. Given the vibrational relaxation time at the picosecond scale [18,19], fast spectral encoding and decoding can be implemented using a wideband infrared pulse and radio-frequency detection without cross-talk. In the current setup employing a QCL array, the spectrum range is limited by the number of excitation sources. This can be further improved by combining arrays covering different IR emission bands, such as 128 channels covering the entire fingerprint region [37]. Other than the QCL array, sources with ultrafast sweeping in nanoseconds-scale, such as midinfrared frequency combs [38] and time-stretched laser pulses [39,40], can also be used for MIRED excitation for further speed improvement. Additionally, the concept of energy deposition detection could theoretically be extended to improve the throughput in other thermal-based spectroscopy methods, such as atomic force microscopy-IR [41,42], which measures near-field thermal effects, fluorescence-detected photothermal microscopy [43,44] for measuring fluorescently labeled organelles, and stimulated Raman photothermal microscopy [45] by employing a fast delay line tuning scheme.

Notably, MIRED spectroscopy offers solution-phase molecular detection where most chemistry and biology occur. In such environments, conventional IR loss measurements require strictly controlled sample thickness and solvent attenuation to collect enough infrared photons on the detector [46]. Using the pump-probe method, MIRED relaxes these conditions by measuring the transient effects occurring precisely at the absorption site. The extension of

time-resolved vibrational spectroscopy in this domain would benefit biological research, aiding in the understanding of chemical reactions involved in cell metabolism and the conformation of biomolecules at the subcellular level—for example, the recently demonstrated use of molecular probes to sense enzymatic reactions via the nitrile group in the cell' s silent window [47]. This technique would enhance quantitative analysis and background correction by enabling the acquisition of the entire spectrum. Additionally, MIRED spectroscopy holds the potential for high-speed midinfrared flow cytometry for screening cells for specific biomolecular markers or the study of the kinetics of rapid reactions in solution [48].

It is noteworthy that the speed of vibrational spectroscopy is ultimately constrained by the number of measurable absorption events occurring upon excitation. MIRED spectroscopy inherently offers higher sensitivity in measuring these events for two main reasons. Firstly, it does not measure the intense excitation field, resulting in a relatively low background compared to direct photon loss measurement [7]. Secondly, sensitivity is enhanced by eliminating the need for midinfrared photon detectors, which typically suffer from thermal noise and low quantum efficiency at high bandwidth. Collectively, transient energy deposition measurement holds the potential for ultrafast vibrational spectroscopy in analysis, where both sensitivity and speed are crucial.

Acknowledgments—This work is supported by NIH Grant No. R35GM136223, R33CA261726, R01 EB032391, R01 EB035429 to J.-X. C. J. Y. developed the MIRED spectroscopy system, designed the experiments, processed the data, and drafted the Letter. C. P., C. T., and D. V. provided the QCL array and technical support. R. B. prepared cancer cell samples. G. C. and X. G. provided the mouse tissue samples. D. D. provided the FTIR measurement. J.-X. C. initialized the project, revised the Letter, and provided scientific guidance. Pendar Technologies has an interest in making the QCL array into a commercial product. J.-X. C. declares a financial interest in Photothermal Spectroscopy Corp., which did not support this work.

The other authors declare no competing interests.

Data availability—The data that support the findings of this article are openly available in Zenodo [49].

[1] A. Gaiduk, M. Yorulmaz, P. Ruijgrok, and M. Orrit, Science **330**, 353 (2010).
[2] S. Adhikari, P. Spaeth, A. Kar, M. D. Baaske, S. Khatua, and M. Orrit, ACS Nano **14**, 16414 (2020).
[3] M. Long, R. L. Swofford, and A. Albrecht, Science **191**, 183 (1976).
[4] S. Berciaud, L. Cognet, G. A. Blab, and B. Lounis, Phys. Rev. Lett. **93**, 257402 (2004).
[5] A. Dazzi and C. B. Prater, Chem. Rev. **117**, 5146 (2017).
[6] D. Zhang, C. Li, C. Zhang, M. N. Slipchenko, G. Eakins, and J.-X. Cheng, Sci. Adv. **2**, e1600521 (2016).
[7] Y. Bai, J. Yin, and J.-X. Cheng, Sci. Adv. **7**, eabg1559 (2021).
[8] J. Yin, M. Zhang, Y. Tan, Z. Guo, H. He, L. Lan, and J.-X. Cheng, Sci. Adv. **9**, eadg8814 (2023).
[9] G. Ishigane, K. Toda, M. Tamamitsu, H. Shimada, V. R. Badarla, and T. Ideguchi, Light Sci. Appl. **12**, 174 (2023).
[10] P. Fu, W. Cao, T. Chen, X. Huang, T. Le, S. Zhu, D.-W. Wang, H. J. Lee, and D. Zhang, Nat. Photonics **17**, 330 (2023).
[11] M. Tamamitsu, K. Toda, M. Fukushima, V. R. Badarla, H. Shimada, S. Ota, K. Konishi, and T. Ideguchi, Nat. Photonics **18**, 738 (2024).
[12] Y. Bai, D. Zhang, L. Lan, Y. Huang, K. Maize, A. Shakouri, and J.-X. Cheng, Sci. Adv. **5**, eaav7127 (2019).
[13] K. Kniazev, E. Zaitsev, S. Zhang, Y. Ding, L. Ngo, Z. Zhang, G. V. Hartland, and M. Kuno, ACS Photonics **10**, 2854 (2023).
[14] T. Yuan, L. Riobo, F. Gasparin, V. Ntziachristos, and M. A. Pleitez, Sci. Adv. **10**, eadj7944 (2024).
[15] J. Zhao *et al.*, Nat. Commun. **13**, 7767 (2022).
[16] M. Tamamitsu, K. Toda, H. Shimada, T. Honda, M. Takarada, K. Okabe, Y. Nagashima, R. Horisaki, and T. Ideguchi, Optica **7**, 359 (2020).
[17] T. L. Bergman, F. P. Incropera, D. P. DeWitt, and A. S. Lavine, *Fundamentals of Heat and Mass Transfer* (John Wiley & Sons, New York, 2011).
[18] X. Chen, Y. Chen, M. Yan, and M. Qiu, ACS Nano **6**, 2550 (2012).
[19] J. C. Lindon, G. E. Tranter, and D. Koppenaal, *Encyclopedia of Spectroscopy and Spectrometry* (Academic Press, New York, 2016).
[20] B. G. Lee *et al.*, IEEE J. Quantum Electron. **45**, 554 (2009).
[21] M. F. Witinski *et al.*, Opt. Express **26**, 12159 (2018).
[22] See Supplemental Material at http://link.aps.org/supplemental/10.1103/PhysRevLett.134.093804 for which includes Refs. [23,24].
[23] I. M. Pavlovetc, E. A. Podshivaylov, R. Chatterjee, G. V. Hartland, P. A. Frantsuzov, and M. Kuno, J. Appl. Phys. **127**, 165101 (2020).
[24] J. Yin, L. Lan, Y. Zhang, H. Ni, Y. Tan, M. Zhang, Y. Bai, and J.-X. Cheng, Nat. Commun. **12**, 7097 (2021).
[25] R. N. Havemeyer, J. Pharm. Sci. **55**, 851 (1966).
[26] A. Idrissi, B. Marekha, M. Kiselev, and P. Jedlovszky, Phys. Chem. Chem. Phys. **17**, 3470 (2015).
[27] V. M. Wallace, N. R. Dhumal, F. M. Zehentbauer, H. J. Kim, and J. Kiefer, J. Phys. Chem. B **119**, 14780 (2015).
[28] D. B. Wong, K. P. Sokolowsky, M. I. El-Barghouthi, E. E. Fenn, C. H. Giammanco, A. L. Sturlaugson, and M. D. Fayer, J. Phys. Chem. B **116**, 5479 (2012).
[29] E. Favaro *et al.*, Cell Metabol. **16**, 751 (2012).
[30] J. Pelletier, G. Bellot, P. Gounon, S. Lacas-Gervais, J. Pouysségur, and N. M. Mazure, Front. Oncol. **2**, 18 (2012).
[31] G. A. Johnson *et al.*, Proc. Natl. Acad. Sci. U.S.A. **120**, e2218617120 (2023).

[32] J. Réhault, F. Crisafi, V. Kumar, G. Ciardi, M. Marangoni, G. Cerullo, and D. Polli, Opt. Express **23**, 25235 (2015).
[33] M. Tamamitsu, Y. Sakaki, T. Nakamura, G. K. Podagatlapalli, T. Ideguchi, and K. Goda, Vib. Spectrosc. **91**, 163 (2017).
[34] C.-S. Liao, P. Wang, P. Wang, J. Li, H. J. Lee, G. Eakins, and J.-X. Cheng, Sci. Adv. **1**, e1500738 (2015).
[35] K. Goda and B. Jalali, Nat. Photonics **7**, 102 (2013).
[36] N. Picqué and T. W. Hänsch, Nat. Photonics **13**, 146 (2019).
[37] C.-S. Liao, R. Blanchard, C. Pfluegl, M. Azimi, F. Huettig, and D. Vakhshoori, Opt. Lett. **45**, 3248 (2020).
[38] D. A. Long, M. J. Cich, C. Mathurin, A. T. Heiniger, G. C. Mathews, A. Frymire, and G. B. Rieker, Nat. Photonics **18**, 127 (2024).
[39] A. Kawai, K. Hashimoto, T. Dougakiuchi, V. R. Badarla, T. Imamura, T. Edamura, and T. Ideguchi, Commun. Phys. **3**, 152 (2020).
[40] K. Hashimoto, T. Nakamura, T. Kageyama, V. R. Badarla, H. Shimada, R. Horisaki, and T. Ideguchi, Light Sci. Appl. **12**, 48 (2023).
[41] J. Chae *et al.*, Nano Lett. **17**, 5587 (2017).
[42] M. Osawa and M. Ikeda, J. Phys. Chem. **95**, 9914 (1991).
[43] Y. Zhang, H. Zong, C. Zong, Y. Tan, M. Zhang, Y. Zhan, and J.-X. Cheng, J. Am. Chem. Soc. **143**, 11490 (2021).
[44] M. Li *et al.*, J. Am. Chem. Soc. **143**, 10809 (2021).
[45] Y. Zhu *et al.*, Sci. Adv. **9**, eadi2181 (2023).
[46] I. Pupeza *et al.*, Nature (London) **577**, 52 (2020).
[47] H. He *et al.*, Nat. Methods, **1** (2024).
[48] R. L. Berger, B. Balko, and H. F. Chapman, Rev. Sci. Instrum. **39**, 493 (1968).
[49] J. Yin, Data for: Mid-Infrared Energy Deposition Spectroscopy, 10.5281/zenodo.12741205 (2025).